Plasma dynamics near critical density inferred from direct measurements of laser hole boring

Chao Gong, Sergei Ya. Tochitsky, Frederico Fiuza, Jeremy J. Pigeon, and Chan Joshi

Phys. Rev. E **93**, 061202 — Published 24 June 2016

DOI: 10.1103/PhysRevE.93.061202

Plasma Dynamics Near Critical Density Inferred from the Direct Measurements of Laser Hole Boring

Chao Gong[1], Sergei Ya. Tochitsky[1*], Frederico Fiuza[2,3], Jeremy J. Pigeon[1], and Chan Joshi[1]

1 Electrical Engineering Department, University of California Los Angeles, Los Angeles, CA 90095

2 SLAC national Accelerator Laboratory, Menlo Park, CA

3 Lawrence Livermore National Laboratory, Livermore, CA

*sergei12@ucla.edu

Abstract

We have used multi-frame picosecond optical interferometry to make direct measurements of the hole boring velocity, v_{hb} of the density cavity pushed forward by a train of CO_2 laser pulses in a near critical density helium plasma. As the pulse train intensity rises, the increasing radiation pressure of each pulse pushes the density cavity forward and the plasma electrons are strongly heated. After the peak laser intensity, the plasma pressure exerted by the heated electrons strongly impedes the hole boring process and the v_{hb} falls rapidly as the laser pulse intensity falls at the back of the laser pulse train. A heuristic theory is presented that allows the estimation of the plasma electron temperature from the measurements of the hole boring velocity. The measured values of v_{hb}, and the estimated values of the heated electron temperature as a function of laser intensity are in reasonable agreement with those obtained from two-dimensional numerical simulations.

PACS: 52.50 Jm, 52.38 Dx, 52.57 Kk

It is well known that a laser pulse of wavelength λ incident on a plasma, will be partially reflected and absorbed once the electron density is close to the critical density, $n_c=1.1 \times 10^{21}$ cm^{-3}/[λ(μm)]^2. If the laser pulse is intense enough, the radiation pressure can steepen [1,2] and push [3,4] the critical density region of an overdense plasma creating a cavity or a hole [3-6]. This happens when the radiation pressure exerted on the critical density layer $P_L=(1+R)I_0/c$ becomes greater than the thermal pressure of the plasma $P_{th}= n_e k_B T_e$. Here R, I_0, n_e and T_e are the plasma reflectivity, laser intensity, electron plasma density and electron temperature, respectively. When $P_L>P_{th}$ stays long enough, the density cavity can be pushed forward in the direction of the laser pulse- phenomenon called laser hole boring (HB) [5]. The HB mechanism is important to a wide range of current plasma research, from radiation-pressure ion acceleration [10,11] to formation of collisionless shocks [12,13] and fast-ignition fusion [7-9].

To date several experiments have purported to measure the HB velocity in solid or foam-target plasmas using a Doppler-shift technique [3,4,14-16]. In those experiments the time integrated [4,15] or time resolved [14,16] Doppler-shift of either the backscattered laser or its self-generated harmonics were used to indirectly infer the velocity of the critical density layer – i.e. without visualization of the radiation pressure-formed cavity in plasma. In other studies the

density cavities produced by intense laser pulses were imaged by X-ray laser pulses [17,18] but probes were too long for time resolved measurements. In fact, no direct measurements of the forward moving overdense ($n_e > n_c$) layer characteristic of HB have been reported in such plasmas, since it is extremely challenging to develop an ultra-fast probe for opaque to light solid-target plasmas.

In contrast to a solid-target plasma, plasma with a peak density of less than a few times n_c (henceforth called a near-n_c plasma) produced by the longer wavelength CO_2 laser, $\lambda = 10.6$ μm ($n_c \sim 10^{19}$ cm^{-3}) in a gas jet is typically transparent to an optical probe, presenting a unique opportunity to study the dynamics of laser HB in time and space simultaneously. In this Rapid Communication we use multi-frame picosecond optical interferometry to make the first direct measurements of the HB velocity v_{hb} of the density cavity pushed forward by a train of CO_2 laser pulses in a near critical density helium plasma. Using a pulse train has allowed us to measure the dependence of v_{hb} on laser intensity and has elucidated the importance of plasma electron heating dynamics during the envelope of the laser macropulse. We show that while the laser pulses push the plasma forward when it is relatively cold, the plasma thermal pressure quickly rises due to the absorption of laser photons in the near-n_c plasma impeding the HB process as the plasma electrons heat up. We present a heuristic theory that allows the temperature evolution in near-n_c plasmas to be calculated using the measured values of the laser intensity and HB velocity. Two-dimensional PIC simulations confirm the observed competition between the laser radiation pressure and the plasma thermal pressure during the laser plasma interaction. Furthermore the electron temperature evolution in the simulations is in reasonable agreement with the temperature inferred when applying the theoretical model to the experimental data. We note that intentional HB using a laser pulse train has been suggested for improving the efficacy of generating hot-electrons in fast ignition fusion [19].

The experiment was carried out at the UCLA Neptune Laboratory that houses a 10 TW class CO_2 laser [20]. In this study, a 10.6 μm wavelength laser beam with an energy up to 50 J was focused by an F/3 parabolic mirror onto a 1.4 mm diameter He gas jet to give a maximum incident $I\lambda^2$ of 2.8×10^{18} W/cm^{-2}μm^2 (normalized laser vector potential $a_0 = eE_o/m\omega c = 1.4$) for the highest intensity micropulse. The FWHM focal spot size was ~50 μm. The ~100 ps long (FWHM) laser macropulse consists of a train of 3 ps micropulses with a bandwidth of ~100 GHz separated by 18.5 ps (see inset box in Fig.1). For probing the plasma, an ~1ps, frequency doubled (532 nm) Nd:glass laser pulse was used in a four-frame interferometer scheme shown in Fig.1. The nearly circularly polarized probe was first sent into a Michelson interferometer where it was split into P- and S- polarization components by use of a Glan-Thompson polarizer. The initial delay for P- and S-components was set up to be 20ps with the P-probe arriving at the CO_2 laser-produced plasma first. Then, both components followed the same optical path and propagated into a Mach-Zehnder interferometer, where the probe was additionally split into two channels separated by a fixed delay of 60ps. The second channel (indicated by a dashed line) probed the plasmas at a 2^o angle from the normal to the CO_2 laser axis. This comb of 1 ps green pulses identified as P1, S1, P2, S2 was 20ps, 40ps and 20ps apart from one another respectively and was then sent through the plasma for probing. A field lens collected the probe beams and polarizing cubes redirected the P- and S-components into four independent CCD cameras. For measurements of HB dynamics on a faster scale, an optical delay (not shown in Fig.1) was mounted in the beam path of channel 1 (solid line in Fig.1) that allowed for generation of a comb

of four pulses separated by 7 ps and covering a~20 ps time window. This four-frame interferometry generated three values of v_{hb} for each laser shot.

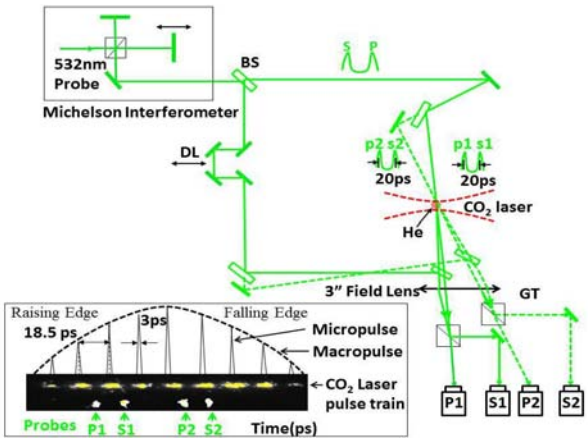

FIG 1. Schematic experimental set-up for four-frame picosecond interferometry. GT is Glan-Thompson polarization cube. DL is an optical delay line. BS is a beam splitter. A temporal profile of a CO_2 laser pulse train and the four green pulses recorded by a streak camera are shown in a box. Also in the box there is a schematic diagram of temporal profile of an envelope of a CO_2 laser macropulse containing a train of micropulses.

Figure 2 shows two of the four interferograms recorded for a 46 J CO_2 laser shot, when the peak neutral density of He was $2x10^{19}$ cm^{-3}. Two frames shown in Fig. 2a and 2b are 20 ps apart with the first frame taken at t=-20ps. Note that in the measurements time t=0 was assigned for the center of the maximum intensity 3 ps micropulse within the CO_2 laser macropulse. Here the 2D projection of this three-dimensional laser-produced density cavity can be clearly seen. The gas jet used in experiment produced a 1.4 mm diameter cylindrical plume where laser interacts with the He gas. Therefore, for the 50 μm spot size of the laser such transverse profile can be considered as flat. The resultant on-axis plasma profiles are plotted in Fig. 2c and 2d [21]. The density profile inside the cavity is steepened compared to the longer density profile upstream of the peak density. Comparison between the frames shows that the peak plasma density is greater in the later interferogram indicating that one additional micropulse has piled up even more plasma density from $n_e=2x10^{19}$ to $2.4x10^{19}$ cm^{-3} (2 to 2.4 n_c). Though the laser could not penetrate the overcritical plasma layer, photoionization and collisional ionization by the electrons accelerated by laser are thought to be responsible for a millimeter-scale exponentially falling density plasma formed on the back of the target [12]. It should be noted that a good agreement between the measured values of plasma density and the initial neutral density indicates single ionization of He atoms in the overall volume of the plasma. This in turn either suggests that the actual average value of a_0 of the most intense micropulse reaching the peak density is ≤1, almost 40% smaller than that of the maximum value determined from the measurement of the laser spot size in vacuum or that He^{2+} may locally being produced within the filamented laser beam but not diagnosable using the interferometry diagnostic.

Using a fiducial placed slightly off the plane of the gas jet, we measured the relative displacement of the maximum density layer in the interferograms. Several slices (fringes) have

been used to accurately measure the position of the peak of the plasma density profile at each frame. For instance, by comparing figures 2a and 2b, one can see that the peak density position has moved by 37±1.5 μm in 20 ps. Thus the velocity of the moving overdense layer is v_{hb} = 1.85x10^{6} m/s or 6.1x10^{-3}c. Moreover the measurements of v_{hb} on the laser axis have revealed that a region with a thickness of ~10λ downstream of the peak density travels with approximately the same velocity. We also measured the longitudinal component of v_{hb} off the laser axis. In the case shown in Fig. 2(a), it decreases slowly reaching v_{hb} = 3x10^{-3}c on the edges of a 45° cone.

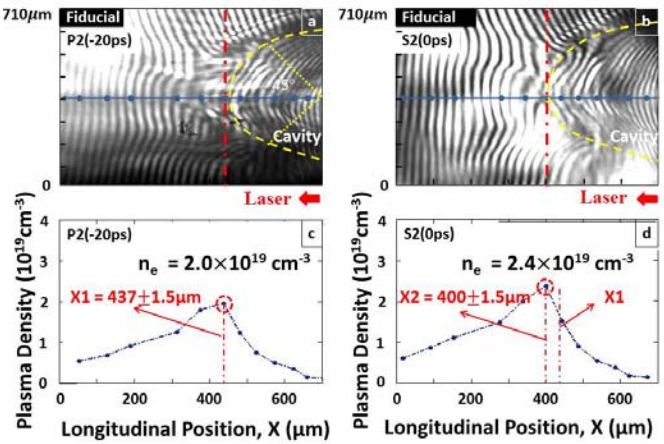

FIG 2.Two of the four interferograms taken for a 46 J CO_2 laser shot (a,b) and the on-axis plasma density profiles extracted from these two frames (c,d) measured at -20 ps (a,c) and 0 ps (b,d) where 0 corresponds to the peak of the laser pulse train. Fig 2(a) shows a 45° cone (dotted lines) used for measurements of HB velocity off-axis. In the figure, the earlier laser micropulses have already produced a parabolic shaped cavity in plasma (indicated by a dashed yellow line). Outside of the cavity there is a higher density ~50 μm thick plasma wall where some blurring of the fringes has occurred due to strong refraction of the probe beams. Therefore, a point-by-point manual analysis of the interferograms [21] has been performed to extract the on-axis plasma density shown by a blue line. The measured uncertainty in plasma density is about 10%.

By varying the time delay between the CO_2 laser and the probe beams, we scanned the fixed comb of green pulses in a t=± 200 ps window. As expected we first observe the onset of HB when the laser intensity exceeds 10^{15} W/cm^{2}, the tunnel ionization threshold for He^{1+}. As seen in Figure 3, the overcritical plasma layer is first pushed by the laser at an increasing speed then begins to slow down past the peak of the macropulse and stops moving altogether at t=60 ps despite the laser still exerting radiation pressure on plasma. As the blue (downward pointed) and the red (upward pointed) triangles show the maximum HB velocity reached is 6.1x10^{-3}c and 3.4x10^{-3}c for the vacuum a_0= 1.4 and 0.6 cases, respectively.

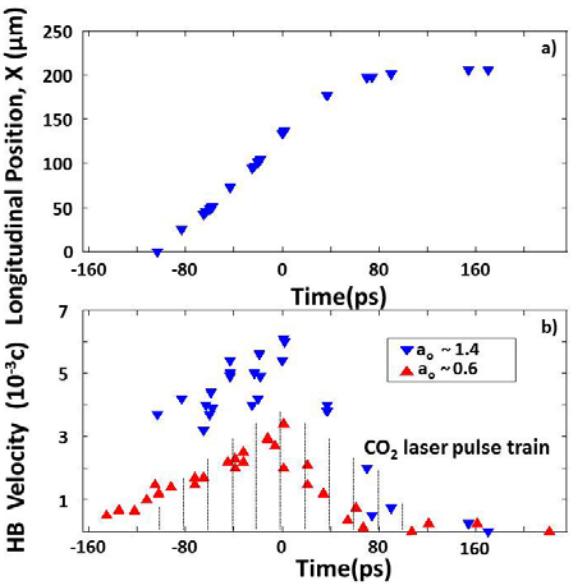

FIG3. (a) Experimentally measured time dependence of the axial position of the maximum plasma density layer for a peak neutral density of 2×10^{19} cm^{-3} and a peak a_0=1.4; (b) the calculated values of the v_{hb} for two different a_0 =1.4 and 0.6 indicated by downward and upward pointed triangles, respectively. The accuracy of velocity measurements in this method of 10% is limited by spatial resolution and error is not shown because it is smaller than the symbol's size.

We observe a striking difference in the variation of v_{hb} during the rising and falling edges of the CO_2 laser pulse train. The HB velocity drops faster during the falling edge of the macropulse and the rate at which this drop occurs depends upon the peak a_0 (see Fig. 3b). We also explored the dynamics of HB between two 3 ps CO_2 laser pulses during the risetime by adjusting the timing between the four probes to be ~7ps. These measurements revealed that within the measurement accuracy, the overcritical plasma layer continued to move between the micropulses at a near constant velocity, i.e. once the plasma ions are set into motion in the forward direction they continue to move until the following (even stronger) laser micropulse arrives.

Figure 4a depicts the measured v_{hb} as a function of the incident I. The first thing to note is that as the laser intensity is increased during the risetime of the laser macropulse (black circles), v_{hb} increases albeit somewhat slower than the cold plasma $I^{0.5}$ scaling [5] (indicated by the solid black curve) and eventually begins to saturate at the highest values of a_0. An important clue as to the dominant physics that determines this scaling of v_{hb} comes from the more rapid decrease of v_{hb} seen during the falling edge of the laser macropulse (blue triangles in Fig. 4a). This hysteresis type behavior is more pronounced at higher laser energy and points to the role of P_{th} working to reduce the efficacy of HB.

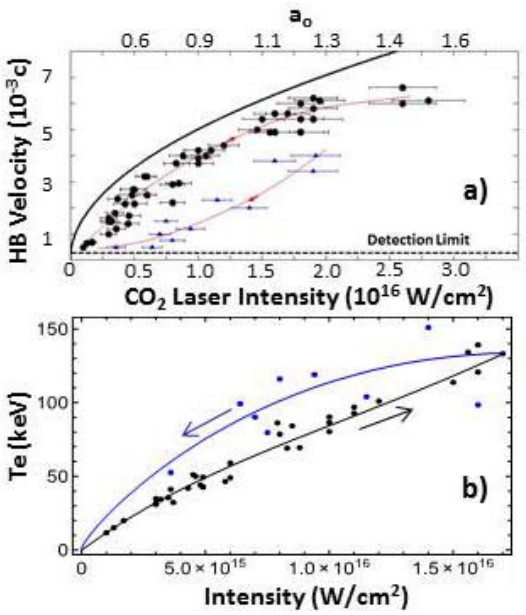

FIG 4. (a) The HB velocity as a function of CO_2 laser intensity for a rising edge (black dots) and falling edge (blue triangles) of the pulse train. Red dashed lines are polynomial fitting to the experimental data with arrows indicating direction of change of laser intensity for rising and falling edges of the CO_2 laser macropulse. The laser intensity values used here are the vacuum values. The error bars of v_{hb} values are small and not plotted. (b) Plasma electron temperature, T_e as a function of the laser intensity deduced from the experimental data points and their fitting curves of the v_{hb} using Eqs. (1) and (2) for the rising edge (black right hand arrow) and falling edge (blue left hand arrow), respectively.

The measured dependence of v_{hb} as a function of laser intensity allows us to infer the plasma temperature evolution using a heuristic theoretical model. This model for HB takes into account both the absorption of laser energy into hot electrons and the effect of plasma pressure on the HB process itself.

We start by calculating v_{hb} from the standard momentum and energy flux conservation equations in the frame of the laser piston, which corresponds to the maximum density layer at which the laser is reflected. Momentum flux conservation is written as $\frac{I_0}{c}(1+R) = P_i + P_e$, where the incident light pressure $\frac{I_0}{c} = \frac{a_0^2}{2} m_e n_c c^2$, the ion momentum flux $P_i = 2n_i(m_i v_{hb})v_{hb}$, and the electron momentum flux $P_e = n_f(m_e \gamma_f v_f)v_f$. Here n_i, and n_f are the background ion density and the laser-heated fast electron density, respectively, and v_f and γ_f correspond to the average fast electron velocity and Lorentz factor. The energy flux conservation is given by $I_0(1-R) = \varphi_i + \varphi_e$, where 1-R is the absorbed fraction of the laser energy, $\varphi_i = n_i(m_i v_{hb}^2)v_{hb}$ is the ion energy flux and $\varphi_e = n_f(m_e(\gamma_f - 1)c^2)v_f$ is the electron energy flux. It is important to note that for $a_0 \sim 1$ and near-n_c plasmas ($n_f \sim 0.1 - 1\, n_e$), $\frac{\varphi_e}{\varphi_i} \approx \left(\frac{m_e}{m_i}\right)\left(\frac{c}{v_{hb}}\right)^3 \gg 1$, implying that the ion energy flux is negligible and that the laser absorption/energy loss is mostly into fast electrons. We can now combine the two equations

above to eliminate R and obtain the HB velocity $v_{hb} = c\sqrt{\frac{Zm_e}{2m_i}\left[a_0^2\frac{n_c}{n_e} - \frac{n_f}{n_e}\left(\gamma_f\frac{v_f^2}{c^2} + (\gamma_f - 1)\frac{v_f}{c}\right)\right]}$.

We note that in the limit where there is no laser energy loss (i.e. no electron heating), R = 1, (n_f= 0, v_f= 0), the second term vanishes and we recover the usual HB velocity given in Ref. 5 and indicated by the solid black line in Fig.4a. In the more general expression derived here, electron heating (given by n_f, v_f) determines the laser absorption coefficient (1-R) and the consequent reduction in HB velocity. Ideally, we would write this energy loss term as a function of the laser a_0 and plasma density, which would lead to a different scaling with a_0. However, determining how n_f, v_f relate to the laser and plasma parameters is not straightforward as it depends on the laser absorption mechanisms which vary as a function of laser intensity and plasma density. For the case of $a_0 \sim 1$ this becomes a particularly difficult problem, where only numerical simulations may help us to understand and approximate these dependences better.

It is now important to consider the role of the fast electrons propagating in the near-n_c target, where $n_e \sim \gamma_f n_c$. In this case because fast electrons will have a density comparable to the background density they will drive a strong and fast return current $v_r = v_f\frac{n_f}{n_e}$, allowing background electrons to be quickly dragged towards the laser to be heated. On top of that heated electrons will reflux in the target [22] and the counter-streaming of electron populations will also contribute to a rapid heating of the target, i.e. the energy directed into fast electrons driven by the laser will be converted to bulk heating of the plasma electrons [23]. Therefore, for near-n_c plasmas we can equate the fast electron energy to the increase in thermal plasma energy or $\frac{n_f}{2}\beta_f^2 = n_e\frac{3}{2}\Delta T_e$, where we have considered non-relativistic electrons, and T_e is in units of $m_e c^2$. In the limit of non-relativistic electrons, $a_0 \lesssim 1$, the HB velocity can then be written as

$$v_{hb} \sim c\sqrt{\frac{Zm_e}{2m_i}(a_0^2 - 3\Delta T_e)} \qquad (1)$$

This expression allows us to relate the HB velocity with the laser parameters and the increase in plasma temperature associated with the energy losses by the laser to heat electrons in near-n_c plasmas. It is important to notice that the temperature increase of the bulk plasma due to laser heating at the surface/critical density is not instantaneous. It occurs on a time scale comparable to the electron recirculation time, $t_r \sim 2\frac{L}{v_f}$, where L is the target thickness. If the laser duration $\tau_L < t_r$ then this bulk heating process will occur on a time scale longer than the laser-plasma interaction, which is the case for each of the micropulses in our experiment. Note that the Spitzer-Braginskii electron-ion collisional time for 100 keV electrons at critical density is about 1 ns, much longer than the electron recirculation time. Thus, during the rising edge of the laser intensity profile, and for initially cold plasmas ($T_{e0} \approx 0$), we can consider that the bulk electron temperature (P_{th}) is not changed significantly during the interaction time (3 ps) of each micropulse. In this case $\Delta T_e \gg T_{e0}$ and we can use Eq. (1) to calculate the increase in plasma temperature during the rising edge of the laser from the measurements of the HB velocity. As the laser reaches its peak intensity, the approximation of a small P_{th} is no longer valid. Now, during the falling edge of the intensity profile, the plasma has already been heated by the high intensity

micropulses, and the temperature increase from the heating due to the later low-intensity micropulses is small compared to the bulk temperature, and we thus neglect it. In this case of a hot plasma we have to take into account the plasma expansion due to its thermal pressure, at the sound speed c_s. This expansion opposes the laser radiation pressure. We approximate the HB velocity for the falling laser edge as a simple balance between these two effects: laser radiation pressure and plasma expansion [24], which leads to

$$v_{hb} \sim c\sqrt{\frac{Zm_e}{m_i}}\left(\frac{a_0}{\sqrt{2}} - \sqrt{T_e}\right) \qquad (2)$$

This allows us to estimate the electron temperature during the falling edge of the laser based again on the measurements of the HB velocity in Fig. 4a. Figure 4b shows the calculated electron temperature by using Eqs. (1) and (2) for the measured values of v_{hb} and a_0 shown in Fig. 4a.We can see that the electron temperature quickly increases during the rising edge of the laser to a peak temperature of ~140 keV. It then slowly decreases during the falling edge of the laser pulse supporting the notion that it is electron heating dynamics that is behind of the observed hysteresis.

The heuristic model presented above neglects many aspects of complex laser-plasma interactions such as plasma formation, underdense plasma heating caused by stimulated Raman scattering [25], laser self-focusing and filamentation, lateral spreading of the hot electrons [26] and the various absorption mechanisms that occur at the critical density itself [6,27,28]. We have therefore performed 2D particle-in-cell (PIC) simulations with the code OSIRIS 3.0 [29]. Below we show that, despite some limitations of the 2D model, it reproduces well the measured values of v_{hb} and the estimated values of T_e using the analytical model. We model the interaction of a train of nine CO_2 laser pulses with a_0 = 0.52, 0.7, 0.85, 0.95, 1.0, 0.95, 0.85, 0.7, 0.52 with an individual pulse duration of 3 ps, pulse separation of 18 ps, and transverse spot size of 84 μm (FHWM), with a He gas having a peak density of 2×10^{19} cm^{-3}. The simulations use a box size of 1.6 mm x 1 mm, a spatial resolution of $\lambda_0/30$ in each direction, and 36 particles per cell per each plasma species. The plasma formation by field ionization of the gas is self-consistently modeled using the ADK tunnel ionization model [30].

The simulation results, summarized in Figure 5, show that the first micropulse with a_0=0.5 tunnel ionizes helium up to the critical density, creating a He^+ plasma. Further ionization of the low-density gas surrounding the interaction region is mediated by the currents associated with energetic electrons that are heated by the laser [24,26]. The train of laser pulses then significantly modifies the plasma profile during its interaction, leading to density steepening near the critical surface, as shown in Fig. 5a for t=0. The lasers strongly filament between 0.5–1.0 n_c, but most of their energy still reaches the critical density region, pushing it forward due to the radiation pressure (Fig. 5b). Such filamentation may be one of the reasons of shot-to-shot scattering of the hole boring velocity data observed in Fig.3b mainly for high-intensity shots. Simulations confirm that the peak of the density profile corresponds to the position and the density where each micropulse is stopped and that the critical density layer continuously moves in between the micropulses as observed in the experiment (Figs. 5c and 5d). The position of the peak density layer (Fig. 5c) as a function of time (peak laser intensity) is in reasonable agreement with the experimental data shown in Fig. 3a and with the theoretical prediction of Eqs. (1)-(2). For a maximum a_0=1.0, the plasma density peaks at 1.6 n_{cr}. The maximum theoretical HB

velocity of $6x10^{-3}c$, is in reasonable agreement with the experimental value of $5.2x10^{-3}$ c and simulation value of $5.8x10^{-3}$. The evolution of the position of peak density and bulk electron temperature confirms that HB is stronger during the rising edge of the pulse train, as observed experimentally. Strong heating of the plasma during the rising edge of the laser works against HB during the falling edge of the laser. It is seen in Fig.5c that the electron temperature T_e reaches ~140 keV at the peak of intensity (t = 0), again consistent with the temperature inferred using the heuristic theory (Fig. 4b). In the theoretical curve we switch from Eq. (1) to Eq. (2) at t=0. Finally we note that despite the complexity of the laser-plasma interaction, the hole boring process appears to be quite robust as the on axis space-time diagram of Fig. 5d shows.

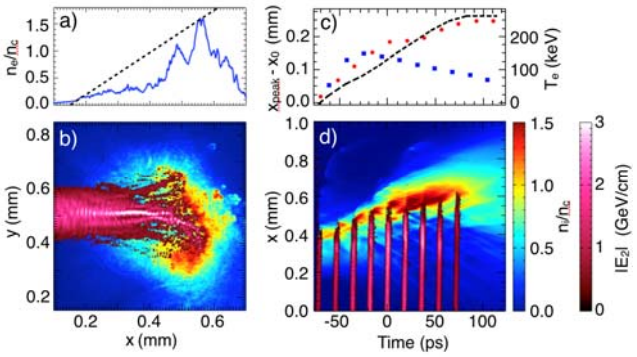

FIG 5. (color) OSIRIS simulation of the interaction of a train of CO_2 laser pulses. **(a)** On-axis plasma density profile at t=0. The initial gas profile is triangular with a 500 μm ramp, corresponding to experimentally measured profile, and is shown by the black dashed line. (b) 2D laser and plasma density profiles at peak laser intensity or t=0 ps. (c) Temporal evolution of the longitudinal position of peak plasma density, X_{peak}-$X_{0,}$ obtained in the simulation (red marks) and from Eqs. (1)-(2) for the laser intensity and electron temperature measured in the simulations (black dashed line). Time dependence of T_e from simulations is shown by blue squares. (d) Space-time diagram of the evolution of the laser field and plasma density on axis.

In summary, by using direct measurements of the HB velocity we have shown that a 10λ thick layer of overdense plasma, once pushed by a laser pulse continues to move between the micropulses due to inertia of ions and that during the risetime of the macropulse, where $P_L>P_{th}$, v_{hb} increases steadily. As plasma electrons are heated P_L/P_{th} rapidly drops during the falling edge of the macropulse causing v_{hb} to decrease more rapidly resulting in a hysteresis behavior. We have presented a heuristic theory that allows the temperature evolution in near-n_c plasmas to be computed as a function of measured laser intensity and v_{hb}. Two-dimensional PIC simulations that take into account the myriad of laser-plasma interaction phenomena are consistent with the observed dynamics of laser HB.

Acknowledgements

Work at UCLA was supported by DOE contract DE-SC0010064 and NNSA grant DE-NA0002950. Simulations were performed on the supercomputers Mira (through INCITE) and Vulcan (through LLNL Grand Challenge). F.F. was supported by the Lawrence Fellowship (LLNL) and by SLAC under the DOE LDRD program. The authors acknowledge the OSIRIS Consortium, consisting of UCLA and IST (Portugal) for the use of the OSIRIS 3.0 framework and the visXD framework.

References

1. R. Fedosejevs, I.V. Tomov, N.H. Burnett, G.D. Enright, and M.C. Richardson, Phys. Rev. Lett., **39**,932 (1977).
2. D.T. Attwood, D.W. Sweeney, J.M. Auerbach, and P.H.Y. Lee, Phys. Rev. Lett., **40**,184 (1978).
3. X. Liu and D. Umstadter, Phys. Rev. Lett., **69**,1935 (1992).
4. M.P. Kalashnikov, P.V. Nickles, Th. Schlegel, M. Schnuerer, F. Billhardt, I. Will, W. Sandner, and N.N. Demchenko, Phys. Rev. Lett., **73**,260 (1994).
5. S.C. Wilks, W.L. Kruer, M. Tabak, and A.B. Langdon, Phys. Rev. Lett., **69**,1383 (1992).
6. Y. Sentoku, W. Kruer, M. Matsuoka, and A. Pukhov, Fusion Science and Technology, **49**, 278 (2006).
7. M Tabak, J. Hammer, M.E. Ginsky, W.L. Kruer, S.C. Wilks, and J. Woodworth, Phys. Plasmas, **1**, 1626 (1994).
8. R. Kodama, H. Shiraga, K. Shigimori, Y. Toyama, S. Fujioka, and H. Azechi, Nature, **418**, 933 (2002).
9. M. Dunne, Nature Phys. **2**, 2 (2006).
10. C.A. Palmer, N.P. Dover, I. Pogorelsky, M. Bazien,. G.I. Dudnikova, M. Ispiriyan, M.N. Polyaskiy, J. Schreiber, P. Shkolnikiv, V. Yakimenko, and Z. Najmudin , Phys.Rev. Lett., **106**,014801 (2011).
11. A. Macchi, M. Borghesi, and M. Passoni, Rev. Mod. Phys. **85**, 751 (2013).
12. D.H. Haberberger, S. Tochitsky, F. Fiuza, C. Gong, R.A. Fonseca, L.O. Silva, W. B. Mori, C. Joshi et al, Nature Phys., **8**, 95 (2012).
13. F.Fiuza, R.A. Fonseca, J. Tonge, W. B. Mori, and L.O. Silva,, Phys.Rev. Lett., **108**, 235004 (2012).
14. R. Kodama, K. Takahashi, K.A. Tanaka, M. Tsukamoto, H. Hashimoto, Y. Kato, and K. Mima, Phys. Rev. Lett., **77**,4906 (1996).
15. M. Zepf, M. Castro-Colin, D. Chambers, S.G. Preston, J.S. Wark, J. Zhang, C.N. Danson, A. Dyson, P. Lee, A.P. Fews, P. Gibbon, S. Moustazis, and M.H. Key, Phys. Plasmas, **3**,3242 (1996).
16. Y. Ping, A.J. Kemp, L. Divol, M.H. Key, P.K. Patel, K.U. Akli, F.N. Beg, S. Chawla, C.D. Chen, R.R. Freeman, D. Hey, D.P. Higginson, L.C. Jarrott, G.E. Kemp, A. Link, H.S. McLean, H. Sawada, R.B. Stephens, D. Turmbull, B. Westover, and S.C. Wilks, Phys. Rev. Lett., **109**,145006 (2012).
17. K. Takahashi, R. Kodama, K.A. Tanaka, H. Hashimoto, Y. Kato, K. Mima, F.A. Weber, T.W. Barbee, Jr., and L.B. DaSilva, Phys. Rev. Lett., **84**,2405 (2000).
18. R.F. Smith, J. Dunn, J. Nilsen, V.N. Shlyaptsev, S. Moon, J. Filevich, J.J. Rocca, M.C. Marconi, J.R. Hunter, and T.W. Barbee, Jr., Phys. Rev. Lett., **89**,065004 (2002).
19. V. Mironov, N. Zaharova, E. d'Humieres, R. Capdessus, and V.T. Tikhonchuk, Plasma Phys. Control. Fusion **54**, 095008 (2012).
20. D.H. Haberberger, S.Ya. Tochitsky, and C. Joshi, Opt. Express, **18**, 17865 (2010).
21. C. Gong,S. Tochitsky, J. Pigeon, and C. Joshi, "Four-frame picosecond interferometry system for probing near critical density CO2 laser-produced plasmas," Proceedings of 16th Advanced Accelerator Concept Workshop, July 13-18, San Jose, USA, 2014
22. P.A. Jaanimagi, N.A. Ebrahim, N.H. Burnett, and C. Joshi, Appl. Phys. Lett., **38**, 734 (1981).
23. F.Fiuza, A. Stockem, E. Boella, R.A. Fonseca, L.O. Silva, D. Haberberger, S. Tochitsky, W. B. Mori, C. Joshi, Phys. Plasmas, **20**, 056304 (2013).
24. M.C. Levy, S.C. Wilks, and M.G. Baring, High Energy Density Physics **9**, 198 (2013).
25. W.L. Kruer, *The Physics of Laser Plasma Interactions* (Westview press, Boulder, Colorado, 2003).
26. N.A. Ebrahim, C. Joshi, D.M. Villeneuve, N.H. Burnett, and M.C. Richardson, Phys. Rev. Letts.**43**, 1995 (1979)
27. D.G. Colombant and W. Manheimer, Phys. Fluids, **23**, 2612 (1980).
28. F. Brunel, Phys. Rev. Lett. **59**, 52 (1987).
29. R.A. Fonseca, L.O. Silva, F. Tsung, V.K. Decyk, W. Lu, C. Ren, W.B. Mori, S. Deng, S. Lee, T. Katsouleas, J.C. Adam, Lect. Notes Comp. Sci. **2331**, 342 (2002).
30. M. V. Ammosov, N. B. Delone, and V. P. Krainov, Sov. Phys. JETP **64**, 1191 (1986).